# Chapter 6

# The formation of second-generation primordial objects

## 6.1 Summary

There has been considerable theoretical debate over whether photoionization and supernova feedback from the first Population III stars facilitate or suppress the formation of the next generation of stars. We present results from an Eulerian adaptive mesh refinement simulation demonstrating the formation of a primordial star within a region ionized by an earlier nearby star. Despite the higher temperatures of the ionized gas and its flow out of the dark matter potential wells, this second star formed within 23 million years of its neighbor's death. The enhanced electron fraction within the HII region catalyzes rapid molecular hydrogen formation that leads to faster cooling in the subsequent star forming halos than in the first halos. This "second generation" primordial protostar has a much lower accretion rate because, unlike the first protostar, it forms in a rotationally supported disk of $\sim 10 - 100$ $M_\odot$. This is primarily due to the much higher angular momentum of the halo in which the second star forms. In contrast to previously published scenarios, such configurations may allow binaries or multiple systems of lower mass stars to form. These first high resolution calculations offer insight into the impact of feedback upon subsequent populations of stars and clearly demonstrate how primordial chemistry promotes the formation of subsequent generations of stars even in the presence of the entropy injected by the first stars into the IGM. This chapter has been previously published as a paper in the Astrophysical Journal [3].

## 6.2 Motivation

Calculations performed by Abel, Bryan and Norman ([39], hereafter referred to as ABN02) show that rapid accretion rates driven by molecular hydrogen cooling cause the formation of solitary massive protostars in the range of 30 to 300 $M_\odot$ in minihalos of $10^5 - 10^6$ $M_\odot$ at redshifts $\gtrsim 20$. Simulations indicate that the hard UV spectra of these $10^5$ K zero-metallicity stars will envelop them in large HII regions several kiloparsecs in diameter [76, 215]. Over the main sequence lifetime of the central star (on the order of 2-6 Myr for the range of $30 - 300$ $M_\odot$) half of the baryons within the minihalo are driven beyond its virial radius by ionized flows that quickly steepen into shocks. These shocks exhibit expansion rates of up to ten times the escape velocity of the halo. After the death of the central star, cooling and recombination are out of equilibrium in the ionized gas, which results in significant electron fractions even after its temperature has dropped to 1000 - 2000 K after 20 - 50 Myr. One dimensional, nonrotating calculations [61] predict two possible fates for the primordial stars themselves: complete destruction by the pair instability (140 $M_\odot < M_* <$ 260 $M_\odot$) which is very energetic and leaves no remnant, or direct collapse to black holes above and below this mass range, with the added possibility of SN-like precollapse mass ejection by pulsational pair instabilities from 100-140 $M_\odot$ stars [60].

An important question is whether later generations of stars can efficiently form in the relatively high temperatures and ionization fractions of the relic HII regions left by the first stars. One analytical study [73] found that the first stars injected sufficient entropy into the early IGM by photoheating and supernova explosions to prevent further local star formation in their vicinity. Lyman-Werner SUV background radiation is also thought to have contributed negative feedback by photodissociating primordial $H_2$ and quenching the molecular hydrogen cooling processes allowing the first stars to form [216, 71]. In this chapter we present fully resolved simulations which show that a second primordial star can form in the relic HII region of an earlier Pop III star. We determine its properties, considering the effect of Lyman-Werner radiation from the resultant black hole assuming accretion rates consistent with the density fields left by ionized outflows from the parent minihalo.

## 6.3 Simulation Setup

We carried out simulations using Enzo, an Eulerian adaptive mesh refinement (AMR) hydrodynamics + N-body code described in Chapter 2. We initialized a box of size $300\,h^{-1}$ kpc at $z = 99$ for a cosmology with $(\Omega_M,\ \Omega_\Lambda,\ \Omega_B,\ h,\ \sigma_8,\ n) = (0.3, 0.7, 0.04, 0.7, 0.9, 1)$. We first ran a simulation with $128^3$ dark matter particles in a $128^3$ root grid with 6 total levels of adaptive mesh, refining on a dark matter overdensity of 4.0. This model was run with dark matter alone in order to identify the most massive halo that evolves in the

simulation volume, which at $z \sim 18$ had a mass $\sim 5 \times 10^5 M_\odot$.

We then re-initialized the calculation in the original simulation volume at $z = 99$ with both baryons and dark matter using a $128^3$ root grid and three static nested subgrids, each of which was twice as refined as its parent grid and was centered on the Lagrangian volume of the peak that later evolved into the identified halo. The effective root grid resolution was $1024^3$ in this volume, which corresponds to a comoving spatial resolution of $\sim 300\ h^{-1}$ pc and a dark matter particle mass of $1.8\ h^{-1}\ M_\odot$ in the most highly refined region. Every dark matter particle that later enters into dark matter halos of interest was within this most highly refined grid at the start of the simulation.

We started the simulation with this set of initial conditions at $z = 99$ and followed the collapse of the first star, which occurred at a redshift of 17.76. As a refinement criteria we used a baryon overdensity of 4.0 and a dark matter overdensity of 8.0. In addition, to ensure appropriate simulation resolution we mandated that the Jeans length must be resolved by at least 16 cells at all times, which exceeds the Truelove criterion by a factor of 4 along each axis [217]. At the collapse redshift the three dimensional structure was resolved with 8727 grids on nine levels containing a total of 49,641,744 unique resolution elements.

To compute the extent of the HII region of the 120 $M_\odot$ Pop III star assumed to form in the collapse, we interpolated the density, energy, and velocity fields from the entire Enzo simulation volume at the formation redshift of this star onto a three dimensional grid of fixed resolution with $256^3$ cells for import into a static radiative transfer code. The code utilizes the ionization front tracking technique of Abel [218] to calculate the boundary of the HII region along rays cast outward from the central star by the adaptive ray tracing technique of Abel & Wandelt [219]. Within the HII region we set the ionization fraction to unity and the $H_2$ and $H^-$ fractions to zero. We assume that the mean energy of ionization for the gas is 2.4 eV, which results in a post-ionization temperature of $\sim 18,000$ K when calculated in our multispecies ZEUS simulations. This is somewhat cooler than one might expect due to the relatively hard spectrum of massive primordial stars, and is a result of our use of monochromatic radiative transfer in the ZEUS code, which underestimates the UV photoheating of the halo by not taking into account contributions from very high energy photons. Whalen et al. [76] show that an increase in post-front temperatures results in somewhat higher sound speeds. These yield higher shock speeds that promote the photoevaporative flow of gas from the halo in which the first star is formed and could in principle affect the dynamics of nearby halos. We show below that in this case the outflow of gas has a negligible effect on the formation of a second primordial star, which suggests that our result is at worst only weakly affected by post-front temperature. Higher post front temperatures will not significantly retard the cooling and recombination crucial to the formation of molecular hydrogen.

We approximated the dynamics of the HII region by imposing the one dimensional velocity, ionization, density and temperature profiles for a 120 $M_\odot$ star at the end of its

main sequence lifetime from Whalen et al. [76] along every line of sight from the central star. We modified baryon densities and velocities out to $\sim 120$ pc (corresponding to the location of the shock wave in the 1D calculation) but changed only ionization fractions and temperatures beyond this radius out to the boundary of the HII region determined by the ray tracing code. We then mapped this HII region onto the full hierarchy of grids in the Enzo calculation, centering it on the location of the first protostar. This state corresponds to only 2.5 million years after the initial star formed ($z \simeq 17.4$), so we assume that instantaneous ionization is a reasonable approximation for all gas outside the first halo (which has had the hydro profiles from the 1D simulations imposed in it). An important question is whether the satellite halos are also ionized by the I-front propagating outward from the first star, an issue investigated in detail at later redshifts by Shapiro et al. [220]. Simulations we performed in 1D in ZEUS-MP indicate that the neighboring halos are photoionized by the parent star by the end of its main sequence lifetime.

We then continued the simulation until the collapse of the next protostar, which occurs at $z = 16.44$, 22.8 million years later. The final time that we analyzed contains 10,710 grid patches on 24 levels with 54,996,560 unique resolution elements. In this calculation we neglect the pulsational pair instability that may eject the hydrogen envelope for this star [60].

As a check on our simulation setup we also ran a simulation where we simply instantaneously ionized the entire simulation volume by raising the baryon temperature to $\sim 10,000$ K and setting ionization fractions to one and $H_2$ fractions to zero. This simulation tests whether the addition of the one dimensional radial profiles from the Whalen et al. [76] calculations changed the properties of the second protostar appreciably. We find that the collapse time and accretion rate of the protostar formed in this simulation are essentially identical to the results of our full setup, and only discuss results from the full setup in the rest of this chapter.

## 6.4 Results

The second primordial protostar forms in a neighboring minihalo approximately 265 proper parsecs from the location of the halo in which the first star formed (and where the HII region originated). The halo in which this second protostar forms was completely ionized by the first star to a temperature of $\sim 1.7 \times 10^4$ K. Due to its relatively high density, the center of this halo cools very rapidly and molecular hydrogen formation is catalyzed by the extremely high electron fraction. After only a few million years the core of the halo has a molecular hydrogen fraction of $\sim 5 \times 10^{-3}$, well above what one would expect for a halo which has not been ionized. This halo is significantly smaller than the first: $\sim 2 \times 10^5$ $M_\odot$ rather than $\sim 5 \times 10^5$ $M_\odot$.

### 6.4.1 Comparison of the First and Second Stars

Figure 6.1 compares the mass accretion times of the initial and second Population III stars formed in this simulation. In addition, this figure shows the mass accretion time of the halo in ABN02 and an estimate of the Kelvin-Helmholz timescale as a function of mass, using values of luminosity and effective temperature taken from Schaerer [59]. The upper and lower dotted lines correspond to an object with constant accretion rates of $10^{-3}$ and $10^{-2}$ $M_\odot$/year, respectively. Our calculation of accretion timescales for the initial protostar agrees well with that of ABN02. The fact that the two results are in good agreement even though the ABN02 calculations assumed a lower baryon fraction supports the analysis of Ripamonti and Abel [47] showing that all mass scales in these calculations are set by molecular physics. Comparison of the accretion rates to the Kelvin-Helmholz timescale provides an estimate of $\sim 200$ $M_\odot$ for the upper bound of the mass of the star. The accretion timescales suggest a reasonable lower bound of $\sim 80$ $M_\odot$, since this much gas will accrete in $10^4$ years, an insufficient time for fusion to begin. In contrast, the accretion rate of the second protostar is over an order of magnitude lower. This is because the second protostar has a much more pronounced thick disk structure than the first protostar. The disk is rotationally supported past a radius $\sim 0.01$ pc (corresponding to an enclosed mass of $\sim 10$ $M_\odot$), whereas the disk around the first star in the volume is not. Similar accretion timescale arguments as before suggest a mass of $\sim 5 - 20$ $M_\odot$ for the second star, although accretion physics will ultimately determine the true mass, particularly given the presence of this more pronounced disk.

Examination of the net angular momentum of the two halos is illuminating. The angular momentum of a cosmological halo can be described by the dimensionless spin parameter: $\lambda \equiv J|E|^{1/2}/GM^{5/2}$ where J is angular momentum, E is the total energy, G is the gravitational constant and M is the halo angular momentum. This is roughly equivalent to the ratio of the angular momentum in the halo to the angular momentum needed for the halo to be completely rotationally supported [123]. Typical values of the spin parameter for cosmological halos are $\sim 0.02-0.1$, with a mean of $\lambda \simeq 0.05$ [221, 222]. We find that the halo in which the first primordial protostar forms has a spin parameter for the gas and dark matter of $(\lambda_{gas}, \lambda_{dm}) = (0.0275, 0.0363)$, which is slightly lower than the mean. The spin parameter of the second halo is $(\lambda_{gas}, \lambda_{dm}) = (0.1079, 0.1607)$, which is atypically high. Examination of the evolution of angular momentum in the gas of the halos as the two protostars form shows that the angular momentum distributions are different in the two clouds, and if angular momentum is conserved one would expect to see a centrifugally supported disk that is approximately four times larger in the second halo.

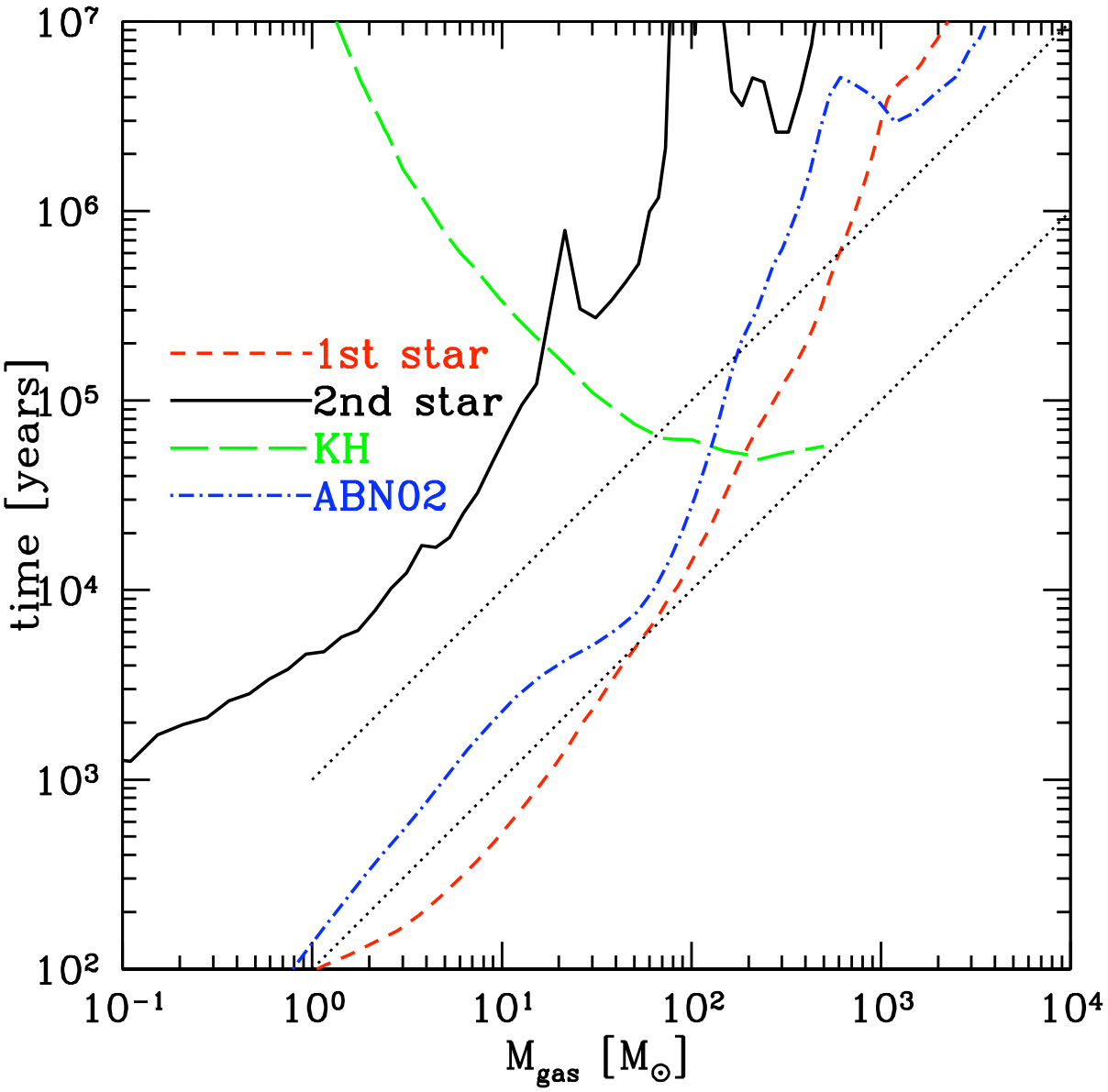


Figure 6.1: Mass accretion time $t_a = M(r)/\dot{M} \equiv M(r)/(4\pi r^2 \rho v_r)$ as a function of enclosed gas mass. This is at the final output corresponding to $z = 16.437$. The dashed line is the corresponding data dump of the initial star which had formed at $z = 17.67$. The red dashed line corresponds to the first star to form in this simulation. The blue dot-dashed line corresponds to the first star calculated in ABN02. The solid black line corresponds to the second star forming in this simulation, and the green long-dashed line corresponds to the Kelvin-Helmholz time of a representative star. The upper and lower black dotted lines correspond to objects with constant mass accretion rates of $10^{-2}$ and $10^{-3}$ $M_\odot$/yr, respectively.

### 6.4.2 Black Hole Accretion

Here we consider whether accretion onto a relic black hole could generate enough photodissociative radiation to inhibit $H_2$ formation in the second star's halo. We assume Bondi-Hoyle accretion [223] for the 120 $M_\odot$ black hole that forms after the collapse of the first star to estimate the Lyman-Werner flux from its accretion. This rate depends on the mass of the accretor as well as the local gas temperatures, densities, and relative velocities it encounters. To sample the local environment the black hole would traverse over the duration of the simulation, we followed the 40 dark matter particles closest to the first protostar (within $\sim 0.1$ proper pc) from the end of its main sequence lifetime until the collapse of the second protostar. We tallied the cell quantities they crossed to compile the accretion rate history each particle would have if it were the black hole. The histories for the 40 black hole proxies appear in Figure 6.2. The mass accretion rates grow from $10^{-11}$ $M_\odot$/yr to $10^{-8.5}$ $M_\odot$/yr for most of the tracer particles.

To estimate the effect of Lyman-Werner radiation from the black hole on molecular hydrogen formation in nearby halos we assume a canonical 10% radiative efficiency for the accretion. The uppermost accretion curve yields $2.2 \times 10^{37}(M/100\ M_\odot)$ erg/s ($\sim 4500\ L_\odot$) for an upper limit to the total luminosity (which is much lower than the Eddington luminosity of this object, $1.5 \times 10^{40}$ erg/s, or $\sim 4 \times 10^6\ L_\odot$). Taking this to be a blackbody spectrum, the flux in the Lyman-Werner band (11.1-13.6 eV) reaching the second protostar is $\sim 1.6 \times 10^{-25}(M/100\ M_\odot)$ erg s$^{-1}$ cm$^{-2}$ Hz$^{-1}$, resulting in photodissociation rates that are significantly lower than the formation rates of molecular hydrogen there. The expulsion of gas by ionized flows from the first halo prevents higher accretion rates and greater Lyman-Werner fluxes. A star in this mass range may shed its envelope just prior to collapse, resulting in a smaller black hole and making the results discussed here an upper limit.

## 6.5 Discussion

This first high resolution three dimensional simulation of the evolution of gas within a primordial HII region demonstrates the crucial role of $H_2$ chemistry driven by photoionization in the formation of the next generation of stars. While this has been addressed in previous work [224] our simulations are the first with sufficient resolution to directly examine the formation of individual protostars. Further investigation will be necessary to determine if the lower accretion rates leading to the smaller mass of the second star are a coincidental feature of this calculation or a general trend of early star formation in halos preprocessed by HII regions. The low accretion rate that we observe in this calculation is primarily due to the high initial angular momentum of the second halo.

One possible source of error lies in the method and assumptions determining whether the neighboring halos are photoionized. While our 1D results indicate that these halos

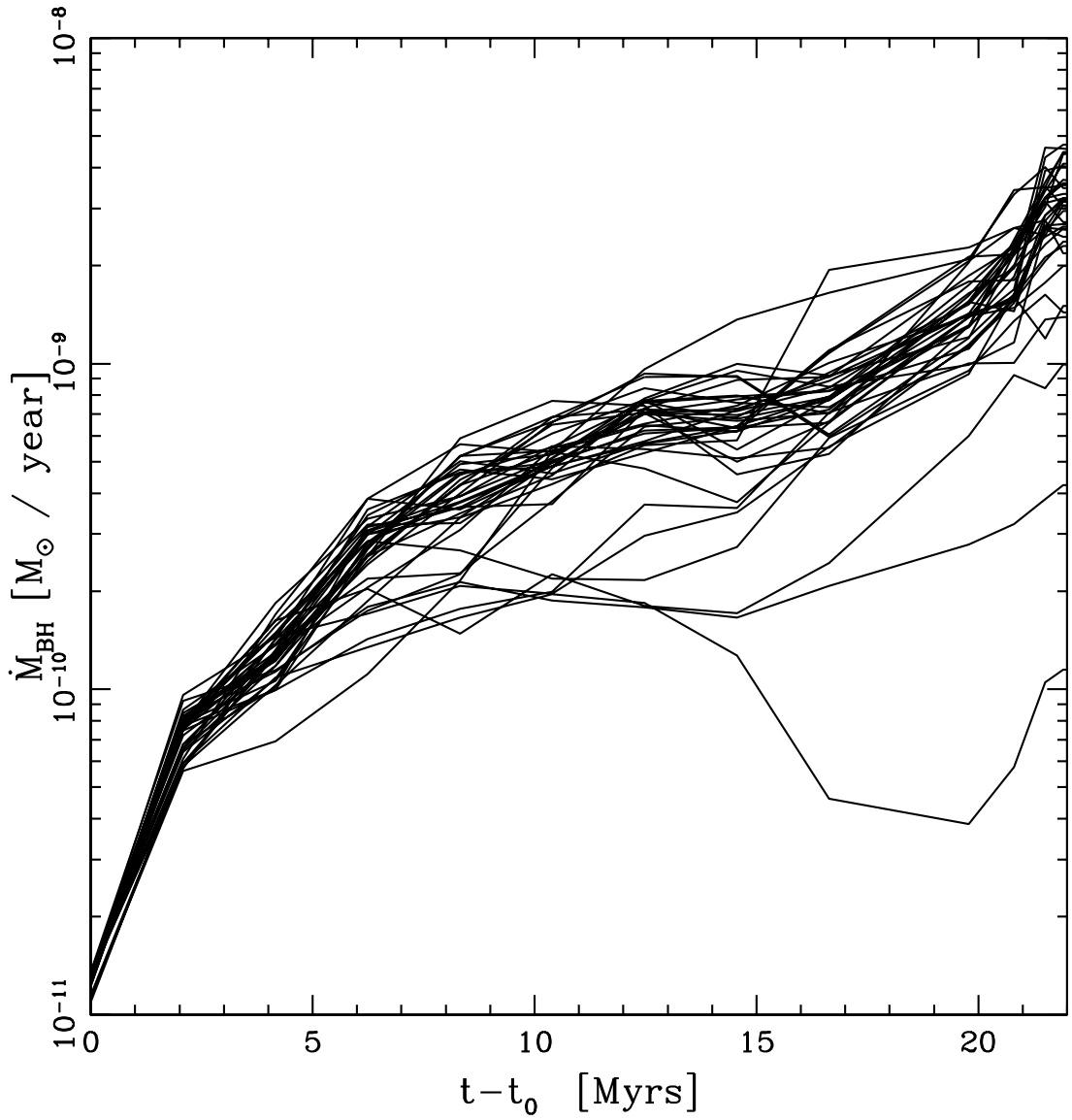


Figure 6.2: Bondi-Hoyle mass accretion rate around the black hole calculated from the local gas temperature, density and relative velocity. Integration of these curves lead to estimates of growth of the black hole (initially 120 $M_\odot$) of that range from 0.009 to 0.032 $M_\odot$ over 23 Myrs

will be ionized, this issue merits further investigation with fully 3D simulations. We further assume that this ionization occurred instantaneously and simply ionize the gas outside of the initial halo without changing the total density or velocity profiles of nearby halos. Instantaneous ionization appears to be a reasonable approximation since the sound crossing time of all of the ionized halos is longer than the main-sequence lifetime of the parent star. Again, full 3D radiation photo-evaporation simulations will be necessary to determine whether the hydrodynamic evolution of these halos during the main sequence lifetime of the parent star is unimportant.

We note that our HII region enveloped roughly a dozen minihalos similar to the one that formed the second star. More calculations will be required to see if these too form stars. The evolution of the massive disk also merits examination to ascertain whether it breaks up into a multiple system or fully accretes to form a single star. The situation realized in our cosmological simulation may lead to objects with initial conditions similar to the cases studied by Saigo et al. [225]. Lower mass second generation stars or the possibility of binaries or multiple systems of primordial stars would have strong implications for the observability of such objects and their impact on subsequent structure formation. Less massive stars might have different nucleosynthetic signatures than those of the pair-instability supernovae that may occur in the first generation of primordial stars. The immense size of early HII regions could also make the scenario of primordial stars forming in a relic HII region much more common than extremely massive stars forming in pristine halos. These two facts taken together may account for the lack of detection of the characteristic odd-even abundance pattern from pair-instability supernovae expected in observations of ultra metal poor halo stars ([226] and references therein). How HII regions from the first stars may regulate local star formation by suppressing the collapse of gas in local halos which have not reached relatively high densities also remains to be explored.